

## Complexation behavior of oppositely charged polyelectrolytes: Effect of charge distribution

Mingtian Zhao, Jihan Zhou, Cuicui Su, Lin Niu, Dehai Liang, and Baohui Li

Citation: *The Journal of Chemical Physics* **142**, 204902 (2015); doi: 10.1063/1.4921652

View online: <http://dx.doi.org/10.1063/1.4921652>

View Table of Contents: <http://scitation.aip.org/content/aip/journal/jcp/142/20?ver=pdfcov>

Published by the AIP Publishing

---

### Articles you may be interested in

[Excluded volume and ion-ion correlation effects on the ionic atmosphere around B-DNA: Theory, simulations, and experiments](#)

*J. Chem. Phys.* **141**, 225103 (2014); 10.1063/1.4902407

[Behavior of rodlike polyelectrolytes near an oppositely charged surface](#)

*J. Chem. Phys.* **124**, 014705 (2006); 10.1063/1.2140692

[Adsorption of oppositely charged polyelectrolytes onto a charged rod](#)

*J. Chem. Phys.* **119**, 8133 (2003); 10.1063/1.1609193

[Polyelectrolyte-macroion complexation. II. Effect of chain flexibility](#)

*J. Chem. Phys.* **115**, 10975 (2001); 10.1063/1.1417508

[Theoretical and experimental adsorption studies of polyelectrolytes on an oppositely charged surface](#)

*J. Chem. Phys.* **110**, 2219 (1999); 10.1063/1.477834

---

An advertisement for AIP Applied Physics Reviews. It features a blue background with a molecular model. On the left, there's a thumbnail of the journal cover showing a grid structure and some text. To the right, the text "NEW Special Topic Sections" is displayed in large white letters. Below that, "NOW ONLINE" is in yellow, followed by "Lithium Niobate Properties and Applications: Reviews of Emerging Trends". At the bottom right is the AIP logo with the text "Applied Physics Reviews".

AIP Applied Physics Reviews

NEW Special Topic Sections

NOW ONLINE

Lithium Niobate Properties and Applications:  
Reviews of Emerging Trends

AIP | Applied Physics Reviews

# Complexation behavior of oppositely charged polyelectrolytes: Effect of charge distribution

Mingtian Zhao,<sup>1,a)</sup> Jihua Zhou,<sup>2,a)</sup> Cuicui Su,<sup>2</sup> Lin Niu,<sup>2</sup> Dehai Liang,<sup>2,b)</sup> and Baohui Li<sup>1,b)</sup>

<sup>1</sup>School of Physics and Key Laboratory of Functional Polymer Materials of Ministry of Education, Nankai University, Tianjin 300071, China

<sup>2</sup>Beijing National Laboratory for Molecular Sciences and the Key Laboratory of Polymer Chemistry and Physics of Ministry of Education, College of Chemistry and Molecular Engineering, Peking University, Beijing 100871, China

(Received 17 February 2015; accepted 13 May 2015; published online 27 May 2015)

Complexation behavior of oppositely charged polyelectrolytes in a solution is investigated using a combination of computer simulations and experiments, focusing on the influence of polyelectrolyte charge distributions along the chains on the structure of the polyelectrolyte complexes. The simulations are performed using Monte Carlo with the replica-exchange algorithm for three model systems where each system is composed of a mixture of two types of oppositely charged model polyelectrolyte chains  $(E\bar{G}E\bar{G})_5/(K\bar{G}K\bar{G})_5$ ,  $(E\bar{E}G\bar{G})_5/(K\bar{K}G\bar{G})_5$ , and  $(E\bar{E}G\bar{G})_5/(K\bar{G}K\bar{G})_5$ , in a solution including explicit solvent molecules. Among the three model systems, only the charge distributions along the chains are not identical. Thermodynamic quantities are calculated as a function of temperature (or ionic strength), and the microscopic structures of complexes are examined. It is found that the three systems have different transition temperatures, and form complexes with different sizes, structures, and densities at a given temperature. Complex microscopic structures with an alternating arrangement of one monolayer of E/K monomers and one monolayer of G monomers, with one bilayer of E and K monomers and one bilayer of G monomers, and with a mixture of monolayer and bilayer of E/K monomers in a box shape and a trilayer of G monomers inside the box are obtained for the three mixture systems, respectively. The experiments are carried out for three systems where each is composed of a mixture of two types of oppositely charged peptide chains. Each peptide chain is composed of Lysine (K) and glycine (G) or glutamate (E) and G, in solution, and the chain length and amino acid sequences, and hence the charge distribution, are precisely controlled, and all of them are identical with those for the corresponding model chain. The complexation behavior and complex structures are characterized through laser light scattering and atomic force microscopy measurements. The order of the apparent weight-averaged molar mass and the order of density of complexes observed from the three experimental systems are qualitatively in agreement with those predicted from the simulations. © 2015 AIP Publishing LLC. [<http://dx.doi.org/10.1063/1.4921652>]

## I. INTRODUCTION

Complex coacervates, formed by associative phase separation of a mixture of oppositely charged species, and the underlying process of co-assembly of oppositely charged species are ubiquitous in natural materials.<sup>1</sup> For example, chromatin is a polyanion–polycation complex of DNA and histones.<sup>2</sup> Furthermore, approaches used in nature are often mimicked with man-made materials to create membranes,<sup>3</sup> vesicles,<sup>4</sup> micelles,<sup>5</sup> and soft gels.<sup>6</sup> The electrostatic assemblies of oppositely charged species have found applications or potential applications in many fields, such as capsules, coating, flocculation, and lubrication.<sup>7–9</sup> Recently, polyelectrolyte complexes (PECs), formed by co-assembly of oppositely charged polyelectrolytes, have attracted a great deal of

interest in designing a novel class of non-viral vectors for gene delivery.<sup>10–13</sup> Numbers of cationic polymers have been developed to condense and encapsulate DNA or RNA.<sup>14–18</sup> Owing to the strong electrostatic interaction, the structures of PECs are governed by many factors, such as charge density, chain length, ionic strength, pH, polymer concentration, salt concentration, solvent quality, chain topology, mixing order, and so on.<sup>19–25</sup> Fine-tuning of these complex structures to meet the needs for their application as new capsules, coatings, or gene deliverers requires detailed knowledge about the structure and the underlying driving forces. Many dynamic and mechanical properties of complex coacervates are closely related to their structure.<sup>26</sup> However, the structure of most complex coacervates is far from understood as summarized recently by Spruijt *et al.*<sup>1</sup> In the present paper, we investigate the complexation behavior and the complex structure of oppositely charged polyelectrolytes in solution.

Small-angle neutron scattering,<sup>27–30</sup> fluorescence recovery after photo-bleaching,<sup>28,31</sup> light scattering,<sup>28</sup> cryo-transmission electron microscopy,<sup>28</sup> rheology,<sup>28</sup> nuclear magnetic

<sup>a)</sup>M. Zhao and J. Zhou contributed equally to this work.

<sup>b)</sup>Authors to whom correspondence should be addressed. Electronic addresses: dliang@pku.edu.cn, Tel./Fax: +86-10-62766170 and baohui@nankai.edu.cn, Tel./Fax: +86-22-23494422.

resonance, and diffusive wave spectroscopy<sup>31</sup> measurements have been used to study properties of complex coacervates formed by oppositely charged species in solution. These studies have improved our knowledge on solution viscosity, sample-averaged diffusion, domain concentrations, etc. Spruijt *et al.* investigated the conformation of single polymer chains and the overall structure of the complex coacervates, formed with a mixture of poly(acrylic acid) and poly(*N,N*-dimethylaminoethyl methacrylate) using small-angle neutron scattering, as well as X-ray scattering and dynamic light scattering.<sup>1</sup> They found that both the polycations and polyanions have an ideal Gaussian chain conformation in the complex coacervates, and that the overall structure is similar to that of a semidilute polymer solution, with the polycations and polyanions strongly overlapping to form a network with a mesh size that is much smaller than the radius of gyration of the polymers. The mesh size decreases with decreasing salt concentration, following a scaling that is in good agreement with predictions from the corresponding salt–polymer phase diagram.<sup>1</sup> It should be mentioned that their samples all have been prepared at quite high salt concentrations, as stressed in their paper,<sup>1</sup> in which the electrostatic interactions are largely shielded. On the other hand, they also observed pronounced deviation from the expected scaling at low salt concentrations, and they declared that additional experiments would have to be done to verify their explanations.<sup>1</sup>

The localizations of the charged units on a polyelectrolyte chain can be expressed as the charge distribution. For a linear polyelectrolyte, the charge distribution along the polymer chain is a fundamental characteristic. It has been found that the binding behavior of cationic polymers with DNA or negatively charged microgels strongly depends on the charge density and the charge distribution of the polycations.<sup>32–35</sup> It is expected that the charge distributions of the oppositely charged polyelectrolytes should have influence on the microscopic structure of the resulting PECs since they affect the electrostatic interactions of the system. Studies of the effect of charge distribution on the microscopic structure of PECs also help to understand many life processes,<sup>2,36,37</sup> as well as the template recognition based on molecular imprinted polymers.<sup>38–40</sup> However, such kinds of studies are rare in the literatures since they are very difficult to be carried out experimentally using synthetic polyelectrolytes due to their polydispersity in nature. The polydispersity in size or in chemical composition introduces extra effects on the complexation process. These effects should be similar to that from changing chain length or charge density, and they are indistinguishable from that generated by the charge distribution. On the other hand, theory and simulation provide an ideal tool for the investigation of the microscopic structure of polymer systems. Especially, advanced simulation techniques, such as Monte Carlo simulations with the replica-exchange (REMC) algorithm<sup>41</sup> have been used for the investigation of the thermodynamic behavior of a strongly charged polyelectrolyte chain with relatively good sampling efficiency.<sup>42,43</sup> The combination of the experimental and simulation work is therefore an effective strategy for the investigation of the microscopic structure of PECs.

In this paper, complexation behavior of oppositely charged model polyelectrolytes in solution is investigated using a

combination of computer simulations and experiments. In our simulations, we design four types of model polyelectrolyte chains which then constitute three model systems to study the effect of charge distribution on the microscopic structure of PECs. All the model chains are of identical lengths and identical average charge densities, and each model system is a mixture of two types of oppositely charged model chains in a solution including explicit solvent molecules. Among the three model systems, only the charge distributions of the two oppositely charged model polyelectrolytes are not identical while other conditions are the same. Simulation results show that both the charge distributions and matching behavior of the charge sequences have significant influence on the complexation behavior and microscopic structures of the resulting PECs at relatively low temperatures which also correspond to polyelectrolyte systems with relatively high ionic strength. Instructed by the simulation results, we design experimental systems based on four types of peptide chains which have identical chain length and identical average charge densities with the model chains. The reason for choosing peptide chains, instead of polyelectrolyte chains, in our experiments is that their chain length and amino acid sequences can be precisely controlled, and hence their charge distribution can be precisely tuned. Therefore, the polydispersity effect of polyelectrolyte chains is avoided. The complexation behavior and complex structures of experimental systems are characterized through laser light scattering and atomic force microscopy (AFM) measurements. The trends of our experimental results are qualitatively in agreement with those from the simulation predictions.

## II. SIMULATION DETAILS

The simulations based on REMC method<sup>41</sup> are applied to a “single-site bond fluctuation” model of polymers.<sup>44</sup> REMC method is a well-known procedure which can achieve good sampling even at low temperatures or for a highly charged system.<sup>42,43</sup> Thus, it may provide high precision for the calculated thermodynamic quantities. Complexation behavior of oppositely charged model polyelectrolytes in a solution including explicit solvent molecules is investigated using REMC simulations. Our previous studies have established that the model and method are appropriate for the study of the thermodynamic behavior of a strongly charged polyelectrolyte chain in solution including explicit solvent molecules.<sup>42,43</sup>

Four types of model chains with each having the same length, the same average charge density, and one of the two charge distributions (one charge for every one neutral spacer and two charges for every two neutral spacer), as listed in Table I, are considered. Each E monomer carries one unit of negative charge, each K monomer carries one unit of positive charge, and all the G monomers are electrically neutral. Three mixture systems are studied, with each composed of equal numbers of two types of oppositely charged model chains in a solution system including explicit solvent molecules. The first mixture system, (EGEG)<sub>5</sub>/(KGKG)<sub>5</sub>, is composed of 20 (EGEG)<sub>5</sub> chains and 20 (KGKG)<sub>5</sub> chains, the second one (EEGG)<sub>5</sub>/(KKGG)<sub>5</sub>, 20 (EEGG)<sub>5</sub> chains, and 20 (KKGG)<sub>5</sub> chains, and the third one (EEGG)<sub>5</sub>/(KGKG)<sub>5</sub>, 20 (EEGG)<sub>5</sub>

TABLE I. List of the designed chains used in the study, where the end groups are occurring only in experimental systems.

Name	Sequence
(KGGG) <sub>5</sub>	Ac-KKGGKKGGKKGGKKGGGG-amide
(KGKG) <sub>5</sub>	Ac-KGKGKGKGKGKGKGKGKG-amide
(EEGG) <sub>5</sub>	Ac-EEGGEEGGEEGGEEGGEEGG-amide
(EGEG) <sub>5</sub>	Ac-EGEGERGEGERGEGERGEGERG-amide

chains, and 20 (KGKG)<sub>5</sub> chains. Therefore, the charge distributions or the charge sequences are the sole factor affecting the complexation of the oppositely charged polyelectrolytes while other conditions are the same.

The simulations are performed on a model system that is embedded in a simple cubic lattice of volume  $V = (L \times c)^3$ , where  $c$  is the lattice constant and  $L$  the number of lattice sites in each side of the simulation box. Each model polyelectrolyte chain is represented as a chain of length  $N = 19$ , including 20 successive beads (monomers) connected by bonds that can adopt lengths of  $c$ ,  $\sqrt{2}c$ , and  $\sqrt{3}c$ . Therefore, each site has 26 nearest neighboring sites. Throughout the simulation, each monomer or each solvent molecule occupies one lattice site. Double occupation of the lattice sites is not allowed. The energetic interaction includes a long-range Coulomb potential and short-range interactions. The Coulomb potential is in the form of  $u_{i,j} = q_i q_j / (Dr_{i,j})$ , where  $q_{i,j} = \pm e$ ,  $D$  is the dielectric constant of the medium, and  $r_{i,j}$  is the distance between two charges. Periodic boundary conditions are utilized and the long-range interactions are computed using an approximation of the Ewald summation.<sup>42,43,45</sup> As the Coulomb interactions are dominating in our system, we set the short-range solvent-monomer and solvent-solvent interactions to zero. Reduced units are used throughout the paper in which the unit of length is  $c$ , the energy is measured in  $e^2/Dc$ , and the temperature in  $e^2/Dck_B$ , where  $k_B$  is the Boltzmann constant.

In the replica-exchange simulation, a set of  $M$  replicas are simulated simultaneously, where the  $i$ th replica is simulated at a unique temperature  $T_i$  ( $i = 1$  to  $M$  and  $T_i < T_{i+1}$ ). The standard Monte Carlo simulations at temperature  $T_i$  are performed and then iterated after each of the replica exchange. When  $N_{MC}$  Monte-Carlo steps are reached, the replica will try to exchange its configuration with one of its two neighboring replicas using the deterministic even-odd scheme.<sup>46</sup> Before sampling,  $5 \times N_{RE}$  attempted replica exchanges have been performed to ensure the equilibrium of the systems. Another  $N_{RE}$  attempted replica exchanges are performed during the sampling.  $N_{RE}$  samples are averaged for the energy and the specific heat curves, and  $N_{RE}/100$  samples are averaged for other quantities. In our simulations,  $L = 40$ ,  $M = 500$ ,  $T_M = 100$ ,  $T_1 = 0.05$ ,  $N_{MC} = 50$ , and  $N_{RE} = 2 \times 10^6$  unless otherwise specified. Simulations with  $N_{RE} = 2 \times 10^7$  have been performed for some cases, and good reproducibility of the structural parameters and thermodynamic quantities is obtained.

The aggregation number (AN) is defined as the average number of chains in one complex. The maximum value of AN is 40 since there are 40 chains in each of our model system. The reduced density ( $\rho$ ) is defined as the ratio of the volume occupied by monomers to that occupied by both

monomers and bounded solvent molecules in a complex. A solvent molecule is considered to be bounded when more than half ( $>13$ ) of its nearest neighboring sites are occupied by monomers. Following Ref. 47, we define asphericity Y as

$$Y = \frac{\lambda_1 - \frac{\lambda_2 + \lambda_3}{2}}{\lambda_1 + \lambda_2 + \lambda_3}, \quad (1)$$

where  $\lambda_{1,2,3}$  are the eigenvalues of the moment of gyration tensor with  $\lambda_1$  being the largest eigenvalue. The moment of gyration tensor  $G$  is

$$G_{\alpha\beta} = \frac{1}{N} \sum_{i=1}^N r_{i\alpha} r_{i\beta}, \quad (2)$$

where  $r_{i\alpha}$  is the  $\alpha$ th component of the position vector  $r_i$ . Asphericity Y is zero for a spherical complex and one for a rodlike complex. For all other shapes, it has a value between zero and one.

### III. EXPERIMENTAL DETAILS

#### A. Materials and preparation

We designed four types of peptide chains with the chain length and charge distribution being the same as those listed in Table I. Lysine (K) and glutamate (E) are employed as positively and negatively charged element, respectively. The neutral spacer, served by glycine (G), does not introduce extra interactions upon complexation. The peptides (purity  $> 99\%$ ) were synthesized by GL Biochem. Ltd. (Shanghai, China), and used without further purification. Trizma® base and EDTA were purchased from Sigma (St Louis, US) and used as received. The stock solutions of the peptides were obtained by dissolving the powder sample with 1 × TE buffer (Tris base: 10 mM, EDTA: 1 mM) buffer. The resulting solutions were diluted by 1 × TE buffer into desired concentrations.

#### B. Laser light scattering (LLS)

A commercialized spectrometer BI-200SM goniometer (Brookhaven Instruments Corporation, Holtsville) was used to perform both static light scattering (SLS) and dynamic light scattering (DLS), over a scattering angular range of 20°–120°. A vertically polarized, 17 mW He–Ne laser (Newport Corporation, CA, US) operating at 633 nm was used as the light source; a BI-TurboCo digital correlator (Brookhaven Instruments Corporation) was used for data collect and process. In SLS, the angular dependence of the excess absolute time-averaged scattered intensity, known as the Rayleigh ratio  $R_{vv}(\theta)$ , was measured. For a very dilute solution, the weight-averaged molar mass ( $M_w$ ) and the root mean-square radius of gyration ( $R_g$ ) were obtained on the basis of

$$HC/R_{vv}(\theta) = (1/M_w)[1 + (1/3)R_g^2 q^2] + 2A_2 C, \quad (3)$$

where  $H = 4\pi^2 n^2 (dn/dc)^2 / (N_A \lambda^4)$  and  $q = 4\pi n / \lambda \sin(\theta/2)$  with  $N_A$ ,  $n$ ,  $dn/dc$ , and  $\lambda$  being the Avogadro's number, solvent refractive index, specific refractive index increment, and wavelength of light in vacuum, respectively. In DLS, the

intensity–intensity time correlation function  $G^{(2)}(\tau)$  in the self-beating mode was measured

$$G^{(2)}(\tau) = A[1 + \beta|g^{(1)}(\tau)|^2], \quad (4)$$

where  $A$  is the measured base line,  $\beta$  is a coherence factor,  $\tau$  is the delay time, and  $g^{(1)}(\tau)$  is the normalized first-order electric field time correlation function.  $g^{(1)}(\tau)$  is related to the line width distribution  $G(\Gamma)$  as

$$g^{(1)}(\tau) = \int_0^\infty G(\Gamma) e^{-\Gamma\tau} d\Gamma. \quad (5)$$

By using a Laplace inversion program, CONTIN, the normalized distribution function of the characteristic line width  $G(\Gamma)$  was obtained. The average line width,  $\bar{\Gamma}$ , was calculated according to  $\bar{\Gamma} = \int \Gamma G(\Gamma) d\Gamma$ .  $\bar{\Gamma}$  is a function of both  $C$  and  $q$ , which can be expressed as

$$\bar{\Gamma}/q^2 = D(1 + k_d C)[1 + f(R_g q)^2] \quad (6)$$

with  $D$ ,  $k_d$ , and  $f$  being the translational diffusive coefficient, diffusion second virial coefficient, and a dimensionless constant, respectively.  $D$  can be further used to obtain the hydrodynamic radius  $R_h$  by using the Stokes-Einstein equation,

$$D = k_B T / 6\pi\eta R_h, \quad (7)$$

where  $k_B$ ,  $T$ , and  $\eta$  are the Boltzmann constant, absolute temperature, and viscosity of the solvent respectively.

For LLS measurements, each of the aqueous sample was passed through a  $0.20 \mu\text{m}$  syringe filter (Sartorius stedim Biotech, Goettingen, Germany) to remove the dust.

### C. Atomic force microscopy

The images were taken in tapping mode using Nanoscope III equipped with a  $110 \mu\text{m}$  scanner (Veeco Instrument, Inc.). Imaging was performed in air with a FESP tip (Bruker instruments, Inc.). The resonant frequency of the cantilever is about  $70 \text{ kHz}$ .  $10 \mu\text{l}$  of the complex solution was deposited on a fresh mica surface using a pipette; the excess solution was blotted away with a strip of filter paper. The sample was washed with Milli-Q water (Millipore, USA) twice to remove salts. It was then air-dried for one day before AFM measurements.

## IV. RESULTS AND DISCUSSION

REMC simulations are carried out to elucidate the effect of charge distribution on the structures of PECs at a molecular level. Results of the structural parameters and thermodynamic quantities for the three mixture systems  $(\text{ECEG})_5/(\text{KGKG})_5$ ,  $(\text{EEGG})_5/(\text{KKGG})_5$ , and  $(\text{EEGG})_5/(\text{KGKG})_5$  are plotted as a function of the inverse of temperature,  $1/T$ , in Fig. 1. At high temperatures ( $1/T < 2$ ), all the curves for the three systems are almost overlapping. This result is reasonable as all the three systems correspond to the same athermal system at a high temperature limit. On the other hand, the different charge arrangements are reflected when the temperature falls. One feature is that the curve for the system  $(\text{EEGG})_5/(\text{KGKG})_5$  is approximately intermediate between the corresponding curves

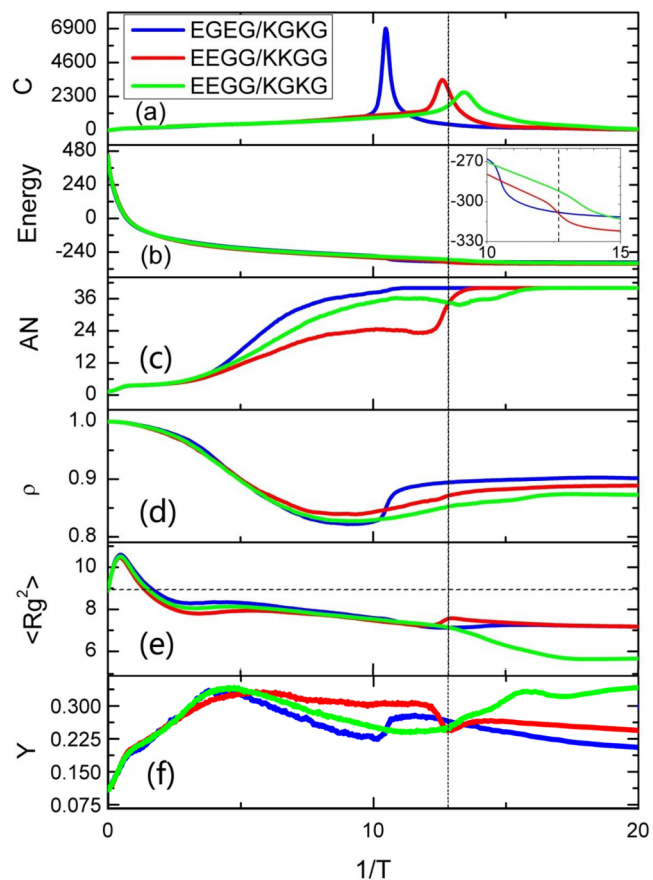


FIG. 1. (a) Specific heat, (b) energy, (c) average aggregation number, (d) reduced density, (e) mean square radius of gyration ( $\langle R_g^2 \rangle$ ), and (f) asphericity as a function of  $1/T$  for the three mixture systems. In Fig. 1(e), the  $\langle R_g^2 \rangle$  value for the corresponding athermal chains are plotted with a horizontal dashed line. The vertical dashed line indicates the temperature of  $T = 0.0778$ .

for the systems  $(\text{ECEG})_5/(\text{KGKG})_5$  and  $(\text{EEGG})_5/(\text{KKGG})_5$  when  $2 < 1/T < 10$ . This result seems reasonable considering that half of the chains in the former system have a charge sequence identical to that for chains in one of the latter two systems, while the other half chains have a charge sequence identical to that for chains in the other system. However, the order of curves among the three systems is totally changed at relatively low temperatures.

In Fig. 1(a), each specific heat ( $C$ ) curve shows a peak. At the temperature corresponding to the peak position of a  $C$  curve, the corresponding energy curve (Fig. 1(b)) and the  $AN$  curve (Fig. 1(c)) all exhibit a relatively large change. All these signals are the characteristics of a phase transition. The peak position in a  $C$  curve, defined as the phase transition temperature, is around  $T \approx 0.0954$ ,  $0.0793$  and  $0.0744$  for systems  $(\text{ECEG})_5/(\text{KGKG})_5$ ,  $(\text{EEGG})_5/(\text{KKGG})_5$ , and  $(\text{EEGG})_5/(\text{KGKG})_5$ , respectively. It is noticed that the phase transition temperatures are quite different for the three systems. For the system  $(\text{EEGG})_5/(\text{KGKG})_5$ , it is not intermediate between those for the systems  $(\text{ECEG})_5/(\text{KGKG})_5$  and  $(\text{EEGG})_5/(\text{KKGG})_5$ , but at a lower temperature than that for any of the latter two systems.

In Fig. 1(c), the three  $AN$  curves are also overlapping at very low temperatures ( $1/T > 16$ ) which corresponds to the state that all the model chains are gathered into one

complex in a model system. It is noticed that in the temperature range where there are pronounced differences among the three curves, the  $AN$  value for the system  $(\text{EGEG})_5/(\text{KGKG})_5$  is always the largest. Furthermore, there exists a small temperature range of 0.0730–0.0778, in which the  $AN$  value follows the sequence as  $AN_{\text{EGEG}/\text{KGKG}} > AN_{\text{EEGG}/\text{KKGG}} > AN_{\text{EEGG}/\text{KGKG}}$ . This order is different from the seemly reasonable order mentioned above. In Fig. 1(d), it is noticed that when  $T < 0.0954$ , the reduced density  $\rho$  value for the system  $(\text{EGEG})_5/(\text{KGKG})_5$  is always the largest, while  $\rho$  value for the system  $(\text{EEGG})_5/(\text{KGKG})_5$  is always the smallest. This order is the same as that for  $AN$  value in the temperature range of 0.0730–0.0778.

Figure 1(e) shows that with decreasing  $T$ , each mean square radius of gyration ( $\langle R_g^2 \rangle$ ) curve increases first, reaches a maximum value, and then decreases. This trend is similar to that obtained for a single polyelectrolyte chain in solution.<sup>42</sup> The increase of  $\langle R_g^2 \rangle$  with decreasing  $T$  (increasing  $1/T$  in Fig. 1(e)) at a high temperature is due to the electrostatic repulsion between charges on the same chain. The increase of  $\langle R_g^2 \rangle$  results in that the total electrostatic interaction of the system decreases with decreasing  $T$ , as shown in Fig. 1(b). As  $T$  is decreased further, the increasing rate of  $\langle R_g^2 \rangle$  with decreasing  $T$  begins to decrease. This is because, with decreasing  $T$ , complexation of the oppositely charged polyelectrolytes sets in, as indicated by the increase in the  $AN$  curve (see Fig. 1(c)) at that temperature range. The increase in the  $AN$  curve also indicates that more chains are in the complexation state with a further decrease in  $T$ , which results in an increase of the electrostatic attraction between the oppositely charged polyelectrolytes. This electrostatic attraction works against the intra-chain electrostatic repulsion between charges on the same chain, and consequently leads to the decrease of the increasing rate of  $\langle R_g^2 \rangle$ , and further leads to the decrease of  $\langle R_g^2 \rangle$ . It is also noticed that the values of  $\langle R_g^2 \rangle$  are slightly lower than the value for the corresponding athermal chains in a relatively wide temperature range ( $2 < 1/T < 8$ ) before the phase transition for all the three systems. Considering that our model chains are mutual- and self-avoiding in such a system, the  $\langle R_g^2 \rangle$  value for the athermal chains should be slightly larger than the value for the ideal Gaussian chain. Therefore, the values of  $\langle R_g^2 \rangle$  for the three model systems should be close to the value for the ideal Gaussian chain in a relatively wide temperature range of  $2 < 1/T < 8$ . This result is quantitatively consistent with the result of a recent paper in which the authors observed that both the polycations and polyanions have an ideal Gaussian chain conformation in the complex coacervates formed with a mixture of poly(acrylic acid) and poly(*N,N*-dimethylaminoethyl methacrylate).<sup>1</sup> On the other hand, it is noticed that in Fig. 1(e), the  $\langle R_g^2 \rangle$  value in system  $(\text{EEGG})_5/(\text{KGKG})_5$  at low temperatures ( $1/T > 14$ ) is much lower than the value for the corresponding athermal chains, hence conformation for chains in this system should be quite different from that for an ideal Gaussian chain at low temperatures. Figure 1(f) shows the asphericity  $Y$  curves which indicate that the complexes formed in all three systems are slightly deviating from spheres, and the deviating degree is a little higher for the complex in system  $(\text{EEGG})_5/(\text{KGKG})_5$  at low temperatures. It should be noticed that the asphericity

defined in Eq. (1) differs from that defined in Ref. 48. However, both of them provide a quantitative measure of the departure from spherical symmetry of a shape. We have compared the results from the two definitions for our system, and find that they have the same tendency (Fig. S1<sup>49</sup>). It is noticed that there is a non-monotonic variation of asphericity with  $1/T$ . This is because that in the intermediate temperature range shown in Fig. 1, there are coexistence of big and small complexes in each system, and the asphericity of a complex depends on its size. This results in that the average asphericity of a system varies non-monotonically.

The results shown in Fig. 1 indicate that at low temperatures, the curve for the system  $(\text{EEGG})_5/(\text{KGKG})_5$  is not intermediate between the corresponding curves for the systems  $(\text{EGEG})_5/(\text{KGKG})_5$  and  $(\text{EEGG})_5/(\text{KKGG})_5$ , suggesting that both the charge distribution and the charge sequence matching of the two oppositely charged polyelectrolytes play important roles in the complexation.

The reason for the difference in the complexation behavior among the three mixture systems should lie in the difference in their complex structures. Figure 2 shows typical snapshots from the simulations for the three systems. It is noticed that the structures in the three systems are quite different at relatively low temperatures. First, as shown in Fig. 2(a) for the  $(\text{EGEG})_5/(\text{KGKG})_5$  mixture at  $T = 0.089$ , all the  $(\text{EGEG})_5$  and  $(\text{KGKG})_5$  chains are aggregated to form a compact complex whose structure is an alternating arrangement of one monolayer of E/K monomers and one monolayer of G monomers. In each E/K monolayer, E and K monomers are alternating with each other. With decreasing  $T$ , the complex structure is similar to that shown in Fig. 2(a), but becomes more and more regular (Figs. 2(b) and 2(c)). Also at  $T = 0.089$ , for the  $(\text{EEGG})_5/(\text{KKGG})_5$  mixture, there sometimes also exists one small complex composed of one  $(\text{EEGG})_5$  chain and one

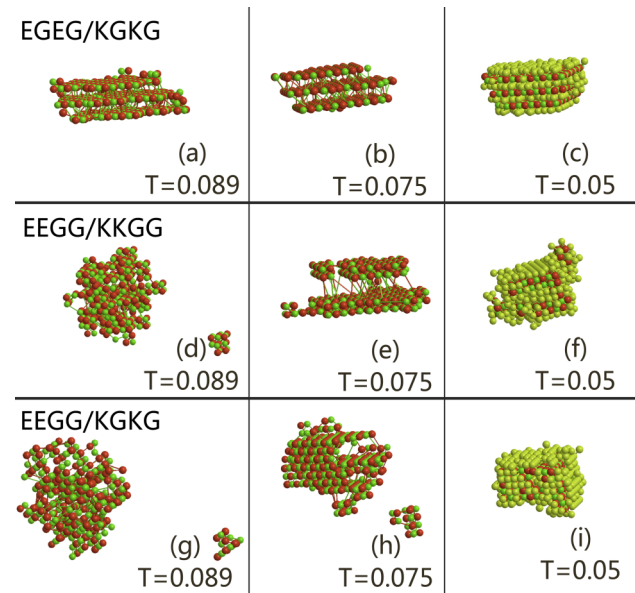


FIG. 2. Typical snapshots from the simulations for polyions in the three mixture systems. The E monomers are shown in green, the K monomers in red, and the G monomers in yellow. In snapshots ((a), (b), (d), (e), (g), and (h)), the G monomers are omitted for clarity.

(KKGG)<sub>5</sub> chain besides a large complex as shown in Fig. 2(d). As the temperature decreases to 0.075, the (EEGG)<sub>5</sub>/(KKGG)<sub>5</sub> mixture gathers into one compact complex (Fig. 2(e)), whose structure is an alternating arrangement of one bilayer of E/K monomers and one bilayer of G monomers. In each E/K monolayer, E and K monomers are alternating with each other. On the other hand, at  $T = 0.089$  and 0.075, there sometimes still exists one small complex formed by one (EEGG)<sub>5</sub> chain and one (KGKG)<sub>5</sub> chain in the (EEGG)<sub>5</sub>/(KGKG)<sub>5</sub> mixture, as shown in Figs. 2(g) and 2(h), since these temperatures are higher than the phase transition temperature of this system. It is interesting to notice that the structure formed by (EEGG)<sub>5</sub>/(KGKG)<sub>5</sub> mixture at low temperatures is not similar to those formed in the other two mixtures. Owing to the mismatched charge sequences, the structure formed by (EEGG)<sub>5</sub>/(KGKG)<sub>5</sub> mixture at  $T = 0.05$  becomes a box in shape whose shell is composed of mixtures of monolayer and bilayer of E/K monomers, while inside the box, there is a trilayer of G monomers and solvents, as shown in Fig. 2(i). As E and K monomers are alternating with each other, solvent molecules are usually associated with G monomers. Hence, the structure with a trilayer G monomers in the (EEGG)<sub>5</sub>/(KGKG)<sub>5</sub> mixture should result in a low density complex, which is consistent with that predicted from the density curves as shown in Fig. 1(d). The compact charge arrangement in (EGEG)<sub>5</sub>/(KGKG)<sub>5</sub> complex (Figs. 2(a)-2(c)) makes it difficult to separate into small complexes. From Figs. 2(c), 2(f), and 2(i), it is noticed that the complex structures at low temperatures are quite different among the three systems. Although this obvious difference occurs at low temperatures, the characteristic of a structure at low temperatures should be somehow reflected at relatively high temperatures. Therefore, the difference in quantities shown in Fig. 1 at both relatively low and high temperatures lies in the difference in their complex structures.

The snapshots before and after the phase transition indicate that the transition corresponds to a process of two or several small complexes gathering into a large complex (Fig. 2). This is consistent with that shown from the AN curves in Fig. 1(c).

In our experimental systems, all the four types peptide chains are in flexible random coil conformation in aqueous solution at pH = 7.4 (Fig. S2<sup>49</sup>). The oppositely charged peptides can interact with each other to form peptide complex in aqueous solution. The size, molar mass, and aggregation number of the complex at  $+/-$  charge ratio = 1 are studied by LLS.

Equal amount of oppositely charged peptides at the same concentration are passed through 0.20  $\mu\text{m}$  syringe filters into dust free vials. The mixture was gently vortexed for 30 s, and then stayed at room temperature for 15 min before the measurement. Figure 3(a) shows the distribution of hydrodynamic radius,  $R_{h,\text{app}}$  (“app” represents apparent) of the peptide complexes at 30°. Similar results are observed at other scattering angles. Only one diffusive mode is observed in all the studied cases. The complexes formed by (EEGG)<sub>5</sub>/(KGKG)<sub>5</sub> mixture, whose charge sequences are mismatched, exhibit relatively narrower distributions in size. Its  $R_{h,\text{app}}$  value is 180 nm, close to that of the complex formed by (EEGG)<sub>5</sub>/

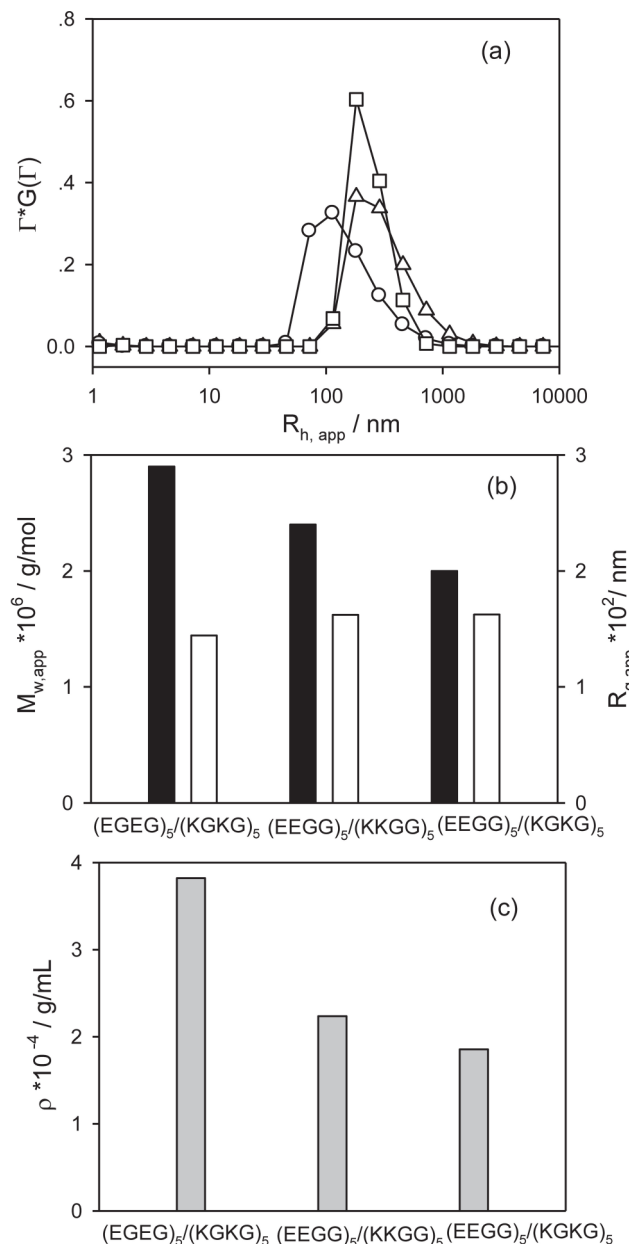


FIG. 3. (a) Size distribution at 30°, (b)  $M_{w,\text{app}}$  (filled column) and  $R_g \times 10^2$  / nm (unfilled column), and (c) density of different peptide complexes. Initial concentrations of both peptides are  $1.0 \times 10^{-4}$  g/ml; charge ratio  $+/- = 1$ .

(KKGG)<sub>5</sub> mixture, but 70 nm larger than the size (about 110 nm) of the complex formed by (EGEG)<sub>5</sub>/(KGKG)<sub>5</sub> mixture. Even though the size of the latter complex is the smallest, its apparent weight-averaged molar mass ( $M_{w,\text{app}}$ ) (the detailed calculation is shown in Fig. S3<sup>49</sup>), as shown in Fig. 3(b), is the highest. The value is  $2.9 \times 10^6$  g/mol, larger than that of the (EEGG)<sub>5</sub>/(KKGG)<sub>5</sub> complex ( $2.4 \times 10^6$  g/mol) and that of the (EEGG)<sub>5</sub>/(KGKG)<sub>5</sub> complex ( $2.0 \times 10^6$  g/mol). The order of  $M_{w,\text{app}}$  among the three systems is qualitatively in agreement with the results of AN values in Fig. 1(c) in the temperature range of  $T \sim 0.0730$ –0.0778, where the AN follows the sequence as  $AN_{EGEG/KGKG} > AN_{EEGG/KKGG} > AN_{EEGG/KGKG}$ . The root mean-square radius of gyration ( $R_g$ ) values are listed in Fig. 3(b), too. The trend of  $R_g$  is similar to that of  $R_{h,\text{app}}$ . The density of the complexes can be obtained

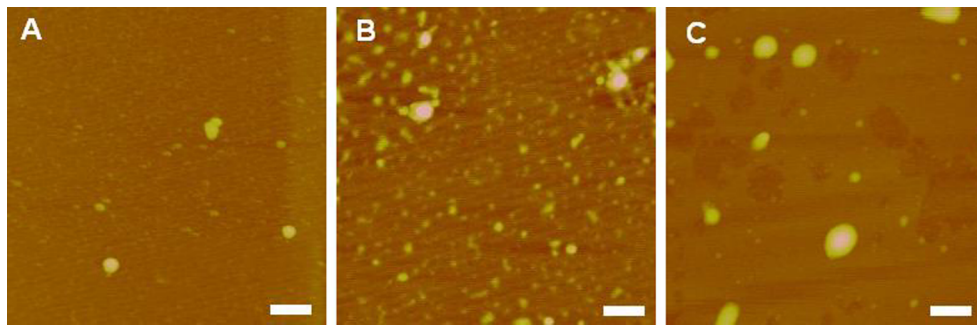
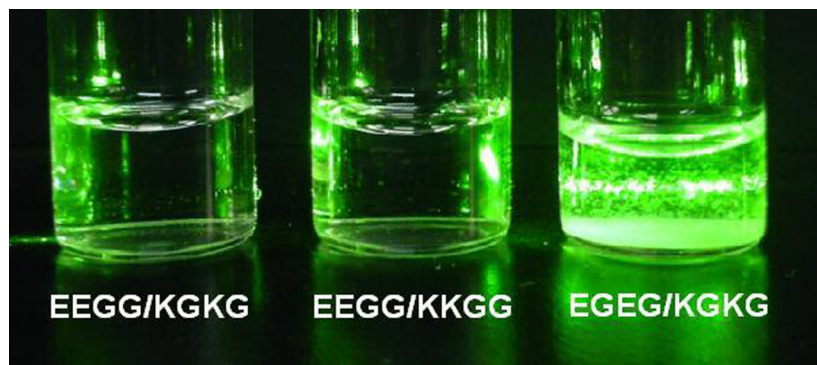


FIG. 4. Morphologies of the peptide complexes formed by (a) (EEGG)<sub>5</sub> and (KKGG)<sub>5</sub>, (b) (EGEG)<sub>5</sub> and (KGKG)<sub>5</sub>, and (c) (EEGG)<sub>5</sub> and (KGKG)<sub>5</sub>. Initial concentration of peptide,  $1.0 \times 10^{-4}$  g/ml; charge ratio: 1. Scale bar: 200 nm.



from  $M_{w,app}$  and  $R_{g,app}$  by  $\rho = 3M_{w,app}/4\pi R_{g,app}^3$ , the magnitude of which follows the order of  $\rho_{EGEG/KGKG} > \rho_{EEGG/KKGG} > \rho_{EEGG/KGKG}$  (Fig. 3(c)).  $\rho_{EGEG/KGKG}$  is about twice  $\rho_{EEGG/KGKG}$ . This result is qualitatively in agreement with the simulation results for the reduced density shown Fig. 1(d), where when  $T < 0.0954$ ,  $\rho_{EGEG/KGKG}$  is always the largest, while  $\rho_{EEGG/KGKG}$  is always the smallest. The above two comparisons suggest that the experimental systems may qualitatively correspond to simulation systems with  $T < 0.0778$ . When  $T < 0.073$ , the identical  $AN$  values in Fig. 1(c) for the three systems are the result a finite system size. Fig. 3 also shows that the size of complexes formed by (EEGG)<sub>5</sub>/ (KKGG)<sub>5</sub> mixture is different from that of complexes formed by (EGEG)<sub>5</sub>/(KGKG)<sub>5</sub> mixture, even though both of them have matched charge sequences and the same charge density.

AFM measurements were also conducted to compare the morphology of the complex on mica surface. The samples were prepared following the same procedure used in LLS. As shown in Fig. 4, almost spherical particles are observed in all the cases. The size of the complex formed by (EGEG)<sub>5</sub>/ (KGKG)<sub>5</sub> mixture (panel (b)) is the smallest. Its size distribution is also the largest, in agreement with the LLS results. The complex formed by (EEGG)<sub>5</sub>/(KGKG)<sub>5</sub> mixture shows a much larger size and a huge abundance on the mica surface. This is probably caused by the aggregation of the complex with mismatched charge sequences on mica surface during the adsorption and drying processes.

At a higher peptide concentration, such as  $5.0 \times 10^{-4}$  g/ml, the complex formed by (EGEG)<sub>5</sub>/(KGKG)<sub>5</sub> mixture is subject to precipitation with time due to its high chain density. As shown in Fig. 5, the flocculation of particles is clearly observed in the laser beam after the peptides are mixed in 4 h.

The solution becomes cloudy. Meantime, heavy precipitates deposit on the bottom of the vial. However, the solutions in other two mixtures are clear under the same conditions (Fig. 5). These results can also be compared with those from the simulations. The results in Figs. 1(c) and 1(d) indicate that complexes formed in the system (EGEG)<sub>5</sub>/(KGKG)<sub>5</sub> have the largest  $AN$  and the largest  $\rho$  values among the three systems in the temperature range of  $0.0730 < T < 0.0954$ . The largest  $AN$  and the largest  $\rho$  may result in a heavy precipitation of the complexes, while the relatively smaller  $AN$  and the smaller  $\rho$  in the other two systems may stay soluble.

## V. CONCLUSION

We have investigated the complexation behavior of oppositely charged polyelectrolytes in a solution using a combination of computer simulations and experiments. We found that both the charge distributions and the matching of the charge sequences have significant influence on the aggregation behavior and the resulting complex microscopic structure. Complex structures with an alternating arrangement of one monolayer of E/K monomers and one monolayer of G monomers, with one bilayer of E and K monomers and one bilayer of G monomers, and with a mixture of monolayer and bilayer of E/K monomers in a box shape and a trilayer of G monomers inside the box are predicted for mixtures of (EGEG)<sub>5</sub>/(KGKG)<sub>5</sub>, (EEGG)<sub>5</sub>/(KKGG)<sub>5</sub>, and (EEGG)<sub>5</sub>/(KGKG)<sub>5</sub>, respectively. For the polyelectrolytes with matched charge sequences, the distribution of neutral spacers is a key factor to tune the size, packing, and density of the resulting complex. Therefore, choosing specific charge sequences and specific distribution of the neutral spacers is able to generate PECs with specific

structures, and hence specific functions. Since PECs have great potential in life science and biomedical fields, our findings not only provide insight into their microscopic structures but also help in designing non-viral vectors for safe and efficient delivery of genes or other cargos.

## ACKNOWLEDGMENTS

The financial supports from the National Natural Science Foundation of China (Nos. 20990232, 21174007, 20990234, 20925414, and 91227121), from the PCSIRT (IRT1257), and from the 111 Project are was greatly acknowledged.

- <sup>1</sup>E. Spruijt, F. A. M. Leermakers, R. Fokkink, R. Schweins, A. A. van Well, M. A. Cohen Stuart, and J. van der Gucht, *Macromolecules* **46**, 4596–4605 (2013).
- <sup>2</sup>N. Korolev, A. Allahverdi, A. P. Lyubartsev, and L. Nordenskiöld, *Soft Matter* **8**, 9322–9333 (2012).
- <sup>3</sup>R. Capito, H. Azevedo, Y. Velichko, A. Mata, and S. Stupp, *Science* **319**, 1812–1816 (2008).
- <sup>4</sup>P. M. Biesheuvel, T. Mauser, G. B. Sukhorukov, and H. Möhwald, *Macromolecules* **39**, 8480–8486 (2006).
- <sup>5</sup>H. M. van der Kooij, E. Spruijt, I. K. Voets, R. Fokkink, M. A. Cohen Stuart, and J. van der Gucht, *Langmuir* **28**, 14180–14191 (2012).
- <sup>6</sup>M. Lemmers, J. Sprakel, I. Voets, J. van der Gucht, and M. Cohen Stuart, *Angew. Chem., Int. Ed.* **49**, 708–711 (2010).
- <sup>7</sup>J. H. E. Hone, A. M. Howe, and T. Cosgrove, *Macromolecules* **33**, 1199–1205 (2000).
- <sup>8</sup>*Macromolecular Complexes in Chemistry and Biology*, edited by P. Dubin, J. Bock, R. Davis, D. N. Schulz, and C. Thies (Springer-Verlag, Berlin, 1994).
- <sup>9</sup>A. F. Thunemann, M. Muller, H. Dautzenberg, J. F. O. Joanny, and H. Lowen, in *Polyelectrolytes with Defined Molecular Architecture II*, edited by M. Schmidt (Springer-Verlag Berlin, Berlin, 2004), Vol. 166, pp. 113–171.
- <sup>10</sup>M. A. Mintzer and E. E. Simanek, *Chem. Rev.* **109**, 259–302 (2009).
- <sup>11</sup>X. Guo and L. Huang, *Acc. Chem. Res.* **45**, 971–979 (2012).
- <sup>12</sup>S. K. Samal, M. Dash, S. Van Vlierberghe, D. L. Kaplan, E. Chiellini, C. van Blitterswijk, L. Moroni, and P. Dubrule, *Chem. Soc. Rev.* **41**, 7147–7194 (2012).
- <sup>13</sup>M. Soliman, S. Allen, M. C. Davies, and C. Alexander, *Chem. Commun.* **46**, 5421–5433 (2010).
- <sup>14</sup>M. E. Davis, J. E. Zuckerman, C. H. J. Choi, D. Seligson, A. Tolcher, C. A. Alabi, Y. Yen, J. D. Heidel, and A. Ribas, *Nature* **464**, 1067–1070 (2010).
- <sup>15</sup>Q. D. Hu, H. Fan, Y. Ping, W. Q. Liang, G. P. Tang, and J. Li, *Chem. Commun.* **47**, 5572–5574 (2011).
- <sup>16</sup>N. P. Gabrielson, H. Lu, L. C. Yin, D. Li, F. Wang, and J. J. Cheng, *Angew. Chem., Int. Ed.* **51**, 1143–1147 (2011).
- <sup>17</sup>D. B. Rozema, D. L. Lewis, D. H. Wakefield, S. C. Wong, J. J. Klein, P. L. Roesch, S. L. Bertin, T. W. Reppen, Q. Chu, A. V. Blokhin, J. E. Hagstrom, and J. A. Wolff, *Proc. Natl. Acad. Sci. U. S. A.* **104**, 12982–12987 (2007).
- <sup>18</sup>S. Bhattacharya and A. Bajaj, *Chem. Commun.* **45**, 4632–4656 (2009).
- <sup>19</sup>H. Dautzenberg, *Macromolecules* **30**, 7810–7815 (1997).
- <sup>20</sup>M. Lemmers, I. K. Voets, M. A. C. Stuart, and J. van der Gucht, *Soft Matter* **7**, 1378–1389 (2011).
- <sup>21</sup>Z. J. Dai and C. Wu, *Macromolecules* **45**, 4346–4353 (2012).
- <sup>22</sup>D. Priftis and M. Tirrell, *Soft Matter* **8**, 9396–9405 (2012).
- <sup>23</sup>D. Storkle, S. Duschner, N. Heimann, M. Maskos, and M. Schmidt, *Macromolecules* **40**, 7998–8006 (2007).
- <sup>24</sup>V. V. Vasilevskaya, L. Leclercq, M. Bousta, M. Vert, and R. Khokhlov, *Macromolecules* **40**, 5934–5940 (2007).
- <sup>25</sup>J. H. Zhou, F. Y. Ke, Y. Q. Xia, J. B. Sun, N. Xu, Z. C. Li, and D. H. Liang, *Polymer* **54**, 2521–2527 (2013).
- <sup>26</sup>E. Spruijt, J. Sprakel, J. M. Lemmers, M. A. Cohen Stuart, and J. van der Gucht, *J. Phys. Rev. Lett.* **105**, 208301 (2010).
- <sup>27</sup>J. H. E. Hone, A. M. Howe, and T. Cosgrove, *Macromolecules* **33**, 1206–1212 (2010).
- <sup>28</sup>A. B. Kayitmazer, S. P. Strand, C. Tribet, W. Jaeger, and P. L. Dubin, *Biomacromolecules* **8**, 3568–3577 (2007).
- <sup>29</sup>S. S. Singh, V. A. Aswal, and H. B. Bohidar, *Int. J. Bio. Macromol.* **41**, 301–307 (2007).
- <sup>30</sup>S. Chodankar, V. A. Aswal, J. Kohlbrecher, R. Vavrin, and A. G. Wagh, *Phys. Rev. E* **78**, 031913 (2008).
- <sup>31</sup>F. Weinbreck, H. S. Rollema, R. H. Tromp, and C. G. de Kruif, *Langmuir* **20**, 6389–6395 (2004).
- <sup>32</sup>E. S. Trukhanova, V. A. Izumrudov, A. A. Litmanovich, and A. N. Zelikin, *Biomacromolecules* **6**, 3198–3201 (2005).
- <sup>33</sup>Y. Ren, X. A. Jiang, D. Pan, and H. Q. Mao, *Biomacromolecules* **11**, 3432–3439 (2010).
- <sup>34</sup>H. Bysell, P. Hansson, and M. Malmsten, *J. Phys. Chem. B* **114**, 7207–7215 (2010).
- <sup>35</sup>K. Mita, M. Zama, and S. Ichimura, *Biopolymers* **16**, 1993–2004 (1997).
- <sup>36</sup>V. A. Belyi and M. Muthukumar, *Proc. Natl. Acad. Sci. U. S. A.* **103**, 17174–17178 (2006).
- <sup>37</sup>P. Carrivain, A. Cournac, C. Lavelle, A. Lesne, J. Mozziconacci, F. Paillasson, L. Signon, J. M. Victor, and M. Barbi, *Soft Matter* **8**, 9285–9301 (2012).
- <sup>38</sup>S. Mallik, R. D. Johnson, and F. H. Arnold, *J. Am. Chem. Soc.* **116**, 8902–8911 (1994).
- <sup>39</sup>M. Kempe and K. Mosbach, *J. Chromatogr. A* **691**, 317–323 (1995).
- <sup>40</sup>A. Bossi, S. A. Piletsky, E. V. Piletska, P. G. Righetti, and A. P. F. Turner, *Anal. Chem.* **73**, 5281–5286 (2001).
- <sup>41</sup>D. J. Earl and M. W. Deem, *Phys. Chem. Chem. Phys.* **7**, 3910–3916 (2005).
- <sup>42</sup>P. Chi, B. Li, and A.-C. Shi, *Phys. Rev. E* **84**, 021804 (2011).
- <sup>43</sup>P. Chi, Z. Wang, Y. Yin, B. Li, and A.-C. Shi, *Phys. Rev. E* **87**, 042608 (2013).
- <sup>44</sup>I. Carmesin and K. Kremer, *Macromolecules* **21**, 2819–2823 (1988).
- <sup>45</sup>J. Klos and T. Pakula, *J. Chem. Phys.* **120**, 2496 (2004).
- <sup>46</sup>M. Lingenheil, R. Denschlag, G. Mathias, and P. Tavan, *Chem. Phys. Lett.* **478**, 80 (2009).
- <sup>47</sup>A. Varghese, S. Vemparala, and R. Rajesh, *J. Chem. Phys.* **135**, 154902 (2011).
- <sup>48</sup>J. Rudnick and G. Gaspari, *J. Phys. A: Math. Gen.* **19**, L191 (1986).
- <sup>49</sup>See supplementary material at <http://dx.doi.org/10.1063/1.4921652> for comparison of asphericity curves calculated from different definitions, CD spectra of four peptides, and calculation of  $M_{w,app}$  and  $R_{g,app}$ .